T. & A.M. Report 350

FRACTURE MECHANICS APPROACH TO ADHESIVE JOINTS

by

G. G. Trantina

Contract No. NOOO19-71-C-0323

Department of the Navy

Naval Air Systems Command

Department of Theoretical and Applied Mechanics

University of Illinois at Urbana-Champaign

Aug, 1971

ABSTRACT

This study investigates the problem of applying fracture mechanics to the opening mode fracture of a two-material (aluminum-epoxy-aluminum) system. The results of a finite element analysis of a two-material, single-edge-notch (SEN) plate are used with a compliance method in order to obtain strain energy rates, $\mathcal{G}$, and with a displacement method to obtain stress intensity factors, K. Approximate relationships between the homogeneous system and the adhesive system for both K and $\mathcal{G}$ are determined. The relationship between K and $\mathcal{G}$ for the adhesive system is obtained. The experimental investigation provides an experimental compliance calibration for the same adhesive system and loading. Good reproducibility of the fracture toughness values obtained for the two-material system with SEN and tapered DCB specimens indicates the geometry independence of the fracture toughness. The effect of the notch root radius and proper specimen preparation are also considered.

ACKNOWLEDGMENT

This investigation was conducted in the Department of Theoretical and Applied Mechanics at the University of Illinois. The author wishes to express his appreciation to his advisor, Professor H. T. Corten, for suggestions, constructive criticism and encouragement. The assistance of H. T. James, Jr. and Mrs. Pat Walker in the preparation of the manuscript is gratefully appreciated.

Financial support for the study has been provided by the Naval Air System Command (Contract No. N00019-71-C-0323).

The results of this investigation will at a later date become part of the author's Ph. D. thesis.

TABLE OF CONTENTS

INTRODUCTION

An adhesive joint consists of two solid materials (adherends) joined by a thin layer of adhesive material which is capable of bonding the adherends together. This definition of an adhesive bond encompasses a number of situations from bonded structural components to fibers bonded together by the matrix in a fibrous composite. Consequently the results of a fundamental study of the fracture behavior of adhesive systems can be applied to a similar range of situations from the fracture behavior of structural components that are bonded together with an adhesive material to debonding at the fiber-matrix interface or separation in the matrix of a composite material.

There are numerous test methods for measuring the strength of adhesive systems. Perhaps more than most other classes of materials, evaluation of adhesives requires specialized test methods. Almost without exception, these methods utilize specimens of various dimensions, shapes and designs prepared specifically to facilitate the test procedure. The resulting data are useful and important in establishing comparative characteristics of adhesives and adhesive joints. However, strength is observed to vary with common joint variables and with the test method.

Many types of flaws are found in both adhesive systems and composites. Voids, foreign matter and small unbonded or weakly bonded regions between constituents as well as mechanical and chemical damage to the constituent materials are inherent to the fabrication process. Service loads and agressive environment combine to cause flaw extension. Observations have shown that these flaws are an important factor in initiating the fracture process particularly for those samples which are on the lower end of the strength or life scatter band. Thus, the fracture behavior should be evaluated by a concept that provides a relationship between the fracture toughness, flaw size, and the applied load. Fracture mechanics provides this relationship. In addition, fracture mechanics provides a test method which

yields a parameter, the fracture toughness, that characterizes the fracture of a material which is essentially independent of the geometry of the test specimen. Fracture mechanics has been extensively applied to linear elastic, isotropic, homogeneous materials. To a lesser extent, bi-material examples composed of two linear elastic, isotropic, homogeneous materials have been studied.

This study investigates the problem of applying fracture mechanics to the opening (tensile) mode fracture of a two-material (aluminum-epoxy-aluminum) system in the form of a bonded joint. A finite element analysis is used to determine the strain energy rates and stress intensity factors for the two-material, single-edge-notch (SEN) system with adhesive layers of various thicknesses. Experimentally, a calibration to determine the strain energy rates for the two-material, SEN system with an adhesive layer of constant thickness was performed. Also, to demonstrate its geometry independence, the fracture toughness was determined for the adhesive system by using specimens of SEN and tapered double cantilever beam geometries.

FRACTURE MECHANICS BACKGROUND

The purpose of fracture mechanics is to characterize the local mechanical behavior at the tip of cracks. A two-dimensional cracked body made of linear elastic material provides the simplest analysis model. In terms of a polar coordinate system (r, θ) with the origin at the crack tip, the elastic state of stress in the vicinity of the crack tip for a homogeneous, isotropic material subjected to mode I (opening) loading is expressed as

$$\sigma_x = \frac{K_I}{\sqrt{2\pi r}} \cos\frac{\theta}{2}\left[1 - \sin\frac{\theta}{2}\sin\frac{3\theta}{2}\right]$$

$$\sigma_y = \frac{K_I}{\sqrt{2\pi r}} \cos\frac{\theta}{2}\left[1 + \sin\frac{\theta}{2}\sin\frac{3\theta}{2}\right] \qquad (1)$$

$$\tau_{xy} = \frac{K_I}{\sqrt{2\pi r}} \sin\frac{\theta}{2}\cos\frac{\theta}{2}\cos\frac{3\theta}{2}$$

where K_I is the stress intensity factor for the opening mode of crack deformation. The stress intensity factor controls the magnitude of the stress field and represents a single parameter characterization of the crack tip stress field. The stress intensity factor is a function of the dimensions of the crack and the cracked body as well as the magnitude and distribution of the applied loads. The displacements in the vicinity of the crack tip for plane strain are:

$$u = \frac{K_I}{G}\sqrt{\frac{r}{2\pi}}\cos\frac{\theta}{2}\left[1 - 2\nu + \sin^2\frac{\theta}{2}\right]$$

$$v = \frac{K_I}{G}\sqrt{\frac{r}{2\pi}}\sin\frac{\theta}{2}\left[2 - 2\nu - \cos^2\frac{\theta}{2}\right] \qquad (2)$$

where G is the shear modulus and ν is Poisson's ratio.

The strain energy rate, $\mathcal{G}$, can be defined in terms related to a method of measurement. Figure 1 shows a cracked elastic body loaded by the force P which causes a displacement of the loading point, e. If the crack extends an incremental

amount, δa, when the load is P_o, the load point will displace an increment, δe, and the load drops off an increment, δP. During this increment of crack extension the strain energy change of the body, δU, is represented by the horizontal cross-hatched region, minus the vertical cross-hatched triangle. Simultaneously an increment of work, δW, equal to $P_o \delta e$ has been done on the body. The strain energy rate is defined as

$$\mathcal{G} = \lim_{\delta A \to O} \frac{\delta W - \delta U}{\delta A} = \frac{dW}{dA} - \frac{dU}{dA} \tag{3}$$

where δA is the incremental area of crack extension equal to the thickness of the body (B) multiplied by δa. With the use of the specimen compliance

$$C = \frac{e_o}{P_o} \tag{4}$$

it can be shown that

$$\mathcal{G} = \frac{P^2}{2B} \frac{dC}{da} \tag{5}$$

One of the uses of this equation is to experimentally determine the strain energy rate for complex systems or structures that have not been treated analytically. The compliance calibration technique (i.e. Eq. 5) requires a value of the load, the thickness of the specimen and dC/da. With a diagram of compliance versus crack length for the specimen of interest, the appropriate tangent $(\frac{dC}{da})$ at a given crack length can be determined and thus the strain energy rate calculated.

For homogeneous materials the stress intensity factor, K, and the strain energy rate, $\mathcal{G}$, are directly related:

$$K^2 = \mathcal{G} E; \text{ plane stress} \tag{6}$$

$$(1 - \nu^2) K^2 = \mathcal{G} E; \text{ plane strain} \tag{7}$$

where E is the modulus of elasticity and ν is Poisson's ratio.

Using fracture mechanics, the resistance of a material to flaw or crack extension can be characterized. Griffith (1) showed that for an ideally brittle material, rapid cracking occurred when the strain energy rate at the crack tip, that is, the amount of energy released per unit area of crack extension, exceeded the surface energy of the newly formed crack. Irwin (2) modified the Griffith criterion by choosing to describe the onset of cracking in a material when the strain energy rate at a crack tip reaches a critical value, $\mathcal{G}_c$ or when the stress intensity at the crack tip attains a critical magnitude, K_c. Irwin's approach does not require a detailed specification of the dissipative processes. $\mathcal{G}_c$ and K_c are essentially independent of geometry and loading conditions and can be considered as a material property that varies with strain rate, temperature, etc. They have the same importance in designing against fracture that yield strength has in designing against flow.

With the two-material adhesive joint system under opening mode loading, observations by this investigator and others (3) have shown that when the bonds were well made, the cracks tend to grow in a center of bond (CoB) fashion. While it is not entirely clear why the crack extends in CoB as compared with extension in the interface region, it is convenient from an analysis point of view to accept this fact. While the adhesive bond is thin, we adopt the attitude that the crack is approximately centered in the adhesive layer, a homogeneous material, between the adherends whose primary role is to impose boundary conditions on the adhesive strip containing the crack.

Previous investigators have studied infinite strips containing longitudinal cracks centered between the boundaries. Paris (4) has described a simple displacement problem where rigid clamps are placed on a stressed (σ) infinite sheet at $y = \pm h$ and a semi-infinite crack is introduced along the x axis from $-\infty$ to the origin. The resulting stress intensity factor is equal to $\sigma\sqrt{h}$. This provides an estimate

of the stress intensity factor for a long thin cracked strip of low modulus material sandwiched between a high (infinite) modulus material. Fichter (5) has analyzed the stresses around the tip of a longitudinal centered finite length crack in an infinite strip produced by pressures and in-plane shearing stresses on the crack face. Knauss (6) has determined the stresses in an infinitely long strip of finite width containing a straight, semi-infinite, centered crack for the case that the clamped boundaries are uniformly displaced normal to the crack. In each of these problems the boundary conditions, either uniform displacements or uniform stresses, simulate adherends that are either rigid or of very low modulus. Combined with the fact that these results are concerned with infinite strips with semi-infinite or finite length cracks, they do not furnish adequate values of the stress intensity factors for the finite width, two-elastic material, SEN plate considered in this paper. Analysis appropriate to this problem will be considered in the next section.

Most of the measurements of the fracture toughness of adhesive joints have been made by Ripling, et al. (3,7-10). They have studied the influence of joint and specimen thickness, strain rate, ambient temperature, humidity, hardener content and post-cure temperature. Stress corrosion cracking, influence of water, crack morphology, crack growth rate, bulk versus bond properties and amine versus anhydride hardeners have also been studied.

FINITE ELEMENT ANALYSIS

The finite element method of stress analysis is applied to a linear elastic, plane problem involving a two-material, single-edge-notch plate (Fig. 2). A discussion of the compliance method used to obtain the strain energy rate, $\mathcal{G}$, and the displacement method used to determine the stress intensity factor, K, follows a brief outline of the general procedure. Then, the relationship between $\mathcal{G}$ and K for the two-material system with a center of bond crack is found.

General Procedure

In structural analysis the finite element method is a well-known stress analysis technique. Structures with complicated geometries, made of several different materials and subjected to various loading conditions can be analyzed with this procedure. First, a continuum is divided by imaginary lines into a number of finite elements interconnected at a finite number of nodes situated on their boundaries. The displacements of the nodes are the basic unknown parameters of the problem. The displacement field within each element is represented as a function of the nodal displacements of that element. The strain-displacement relationships determine the state of strain within the element. The state of stress is obtained by using the appropriate stress-strain relationship. The stiffness matrix and hence the force-displacement relationship for the individual elements is determined by the principle of virtual work. The boundary conditions for the entire structure consist of either the displacements of the boundary nodes or a system of forces concentrated at the nodes and in equilibrium with the boundary stresses and distributed loads. Then, the behavior of the entire structure composed of the individual elements is obtained by using the direct stiffness analysis (11). This behavior is represented by a force-displacement relationship involving the structural stiffness matrix. The details of the finite element method are contained in Ref. (11).

For the present finite element analysis, a six-node triangular element (Fig. 3) was used. The nodes are located at the vertices and the midpoints of the sides of the triangle. Since a second order displacement function is used, a state of linear strain within the elements exists. All numerical computations were done on an IBM 360/75 computer.

The finite element method has been successfully applied to problems in fracture mechanics (12-14). Four specific computational methods for determining stress intensity factors from the finite element results have been used: (1) displacement method, (2) stress method, (3) J-integral method, and (4) compliance method. The first two methods utilize the crack tip displacement and crack tip stress equations respectively. Of these two procedures, the displacement method is preferable because of its simplicity and accuracy. The finite element procedure directly determines the nodal displacements required for the displacement method. With the stress method the finite element analysis does not provide an accurate representation of the large stress gradients very close to the crack tip. The J-integral method requires the evaluation of the appropriate energy density, tractions and displacements. This path independent line integral can be evaluated along a path well removed from the crack tip where the linear strain elements are expected to give accurate results. The compliance method is discussed in the next section.

Compliance Method

Utilizing the displacements from the finite element analysis, the compliance method is used to evaluate the strain energy rates in a manner similar to an experimental compliance calibration. Since the plate in Fig. 2 is symmetrical about a horizontal line coincident with the crack, only the upper half of the plate needs to be analyzed (Fig. 4). The crack length is a and the vertical length of the material in which the crack is embedded is $2L$. The plate has unit thickness, H is 15 units and W is 10 units.

The finite element grid pattern is generated by first locating all nodes at both ends of the radial lines and at the intersection of the radial lines and the material interface. The first ring (semi-ring) of nodes is .0001 units from the actual crack tip. The resulting hole at the crack tip simplifies the nodal numbering system and consequently reduces the band width of the structural stiffness matrix which reduces computer storage space. Also, this avoids the problem of accurately representing the material behavior at the crack tip. The second ring of nodes is located .01 units from the first ring of nodes. The remaining nodes are generated with an arithmatic progression where d is the common difference which is determined by knowing the length of the first division (.01 units), the number of divisions, and the total length of the line segment. The third ring of nodes is .01 + d from the second ring, the fourth ring is .01 + 2d from the third ring, etc. The rings of nodes are joined by straight line segments which divide the plate into quadrilaterals which are then divided into triangles (Fig. 4). Thus, a grid pattern with 273 nodes and 120 elements is generated where the density of elements increases as the crack tip is approached.

The upper boundary of the plate is loaded by a uniformly distributed vertical stress which is equivalent to a system of forces concentrated at the nodes. The total force along the boundary of an element is proportioned with 1/6 at each of the vertex nodes and 2/3 at the midpoint node. This proportioning satisfies not only the static equilibrium requirement but also the requirement that the work done by the distributed system is equal to the work done by the system of nodal forces and displacements. The two vertical boundaries, the crack face and the first ring of nodes are force free. The vertical displacements and horizontal forces of the nodes at and between the points labeled A and B in Fig. 4 are zero. To prevent rigid body motion, the horizontal displacement of the node at point B is also zero.

To obtain a check on the finite element procedure and the compliance method, the strain energy rates were determined for a one-material, single-edge-notch

tension plate. For the plate in Fig. 4, every element was assigned the same elastic properties, the plate was loaded, and the displacement of every node was computed by the finite element procedure. Since the variation of the nodal displacements across the upper boundary was linear but non-uniform, the average nodal displacement was divided by the applied load to determine the compliance of the plate at that particular crack length. After evaluating the compliance over a range of crack lengths, the compliance derivative, dC/da, which is directly related to the strain energy rate (Eq. 5), was evaluated with the use of a movable strip and least squares technique (15). With this technique a function is chosen that can be fitted in a least squares manner to each of a collection of data point sets. After an evaluation and resmoothing operation, the data point set functions are differentiated and a polynomial function is fitted in a least squares manner to the discrete, estimated compliance derivatives. Thus, a smooth compliance derivative versus crack length curve is generated. A combination of 5th thru 11th order polynomials was used with five points per data point set. The results of this procedure for the one-material, single-edge-notch plate are shown in Fig. 5. The dimensionless stress intensity parameter, $\frac{K^2B^2W}{P^2}$, is directly related to the compliance derivative thru the expression:

$$\frac{K^2B^2W}{P^2} = \frac{BEW}{2}\left(\frac{dC}{da}\right) \tag{8}$$

which is obtained from Eqs. 5 and 6. Over a large range of relative crack lengths from .05 to .45, the finite element results differ with the boundary collocation results of Gross, Srawley and Brown (16) by less than 3%.

The same procedure was used to evaluate the compliance derivatives for the two-material, single-edge-notch plate. Figure 6 illustrates the relationship between the compliance derivative and the crack length at various thicknesses (2L) of the adhesive material in which the crack is embedded. The adhesive material has a modulus

of elasticity of 0.5×10^6 psi and the adherend material has a modulus of 10×10^6 psi, approximately that of epoxy and aluminum respectively. Poisson's ratio for both materials is 0.333. For easier comparison of the curves, the results were displayed on a log-linear graph. The lower curve, $L/W = 0$, represents the extreme condition when the plate consists of only the adherend material. The upper line, $L/W > 1$, represents the other extreme condition when the adhesive material is of sufficient thickness such that the influence of the adherend material on the compliance derivative is negligible. The smallest value assigned to L/W was 0.01 since the grid pattern became distorted and ineffective as L became very small.

Figure 7 shows dC/da as a function of L/W for various values of a/W. Since these curves are almost linear over this range, the proper compliance derivative for a plate with a very thin layer of adhesive material can be obtained by interpolation. Since many adhesive systems are characterized by very thin adhesive layers, it is important to note that the strain energy rates for two-material systems, $\mathcal{G}_{A1\text{-}Ep}$, with very thin adhesive layers are closely approximated by the one-material strain energy rates, $\mathcal{G}_{A1}(L/W = 0)$; that is, for L/W very small,

$$\mathcal{G}_{A1\text{-}Ep} \cong \mathcal{G}_{A1} \tag{9}$$

Displacement Method

The stress intensity factors, K_I, for the two-material, single-edge-notch plate are determined with the displacement method. The plane strain y-displacement of the crack surface ($\theta = \pi$ in Eq. 2) in the vicinity of the crack tip is

$$v = \frac{4K_I}{E} \sqrt{\frac{r}{2\pi}} (1 - \nu^2) \tag{10}$$

where E is 0.5×10^6 psi and ν is 0.333. The y-displacement, v, of all of the nodes along the crack face was computed by the finite element program; therefore, the stress intensity factor can be calculated from the displacements at each of these nodes.

Figure 8 shows the stress intensity factors calculated for the one-material, single-edge-notch plate. The previous results for this system (Fig. 5) are indicated on the ordinate ($r/a = 0$) while the remaining points represent values of K_I calculated from the nodal displacements for $r/a > 0$. As $r/a \rightarrow 0$ the displacement equation becomes more accurate but the finite element results become less reliable. Consequently, the method involves an extrapolation of the calculated values of K to the crack tip, ignoring those points too near the crack tip that are obviously in error. Using the extrapolation procedure of Fig. 8 as a pattern, the displacement method was used to determine the stress intensity factors for the two-material system. These results are discussed in the next section.

Comparison of $\mathcal{G}$ and K

The displacement method was used to evaluate the stress intensity factors, K, for the same relative adhesive thicknesses and crack lengths for which the strain energy rates, $\mathcal{G}$, were determined. The two parameters, K and $\mathcal{G}$, are compared using the ratio, $K^2/\mathcal{G}$, versus the relative adhesive thickness (Fig. 9). The average value of the ratio $K^2/\mathcal{G}$ for three representative crack lengths was used for clarity. The resulting step function indicates the following relationship for the two-material system when the modulus of the adhesive material is used ($E_{Ep} = 0.5 \times 10^6$ psi):

$$K^2_{A1\text{-}Ep} = \mathcal{G}_{A1\text{-}Ep} E_{Ep} \tag{11}$$

where $K_{A1\text{-}Ep}$ and $\mathcal{G}_{A1\text{-}Ep}$ are the two-material stress intensity factor and strain energy rate, respectively. Of course, for the one-material system (L/W = 0), the usual plane stress relationship holds:

$$K^2_{A1} = \mathcal{G}_{A1} E_{A1} \tag{12}$$

where $E_{A1} = 10 \times 10^6$ psi.

For the situation of a very thin adhesive layer the approximation of Eq. 9 can be combined with the previous two equations with the result that

$$\left(\frac{K_{A1}}{K_{A1\text{-}Ep}}\right)^2 \cong \frac{E_{A1}}{E_{Ep}} \tag{13}$$

for L/W very small. Consequently, when the crack tip is embedded in a very thin adhesive layer midway between the adherends, its stress intensity can be simply related, thru the ratio of the modulii of elasticity of the adherend and adhesive materials, to the stress intensity factor for a one-material (adherend) system.

EXPERIMENTAL PROGRAM

An experimental investigation was performed to provide an experimental compliance calibration for the two-material, single-edge-notch plate under opening mode loading. Fracture toughness values were measured for the two-material system by using a single-edge-notch plate and tapered double cantilever beam specimens. Other areas of consideration include the specimen preparation and the effect of the notch root radius.

Specimen Preparation

The single-edge-notch specimen positioned in the specimen preparation fixture is shown in Fig. 10. One-half inch thick 2024-T351 aluminum adherends were first degreased with trichloroethylene and then etched in a hot sulfuric acid-sodium dichromate bath. After rinsing with distilled water and air drying the adherends were shimmed, supported and taped to form a 0.01-inch thick cavity for the adhesive (Fig. 10). To aid in the pouring procedure and to remove bubbles in the adhesive, the adherends were placed on a hot plate at 150^{o}F, and the adhesive was heated to 110^{o}F. The adhesive consisted of 10 parts by weight TEPA hardener mixed with 100 parts by weight Dow 332 epoxy resin. Gelation occurred about an hour after pouring and the specimens were then post-cured for five hours at 180^{o}F.

Effect of Notch Root Radius

Experience has shown that the effect of the notch root radius is an important consideration in an adhesive joint study. The effect of notch root radius on the fracture toughness has been investigated. Data from several aluminum alloys (17) indicates that above K_c a proportionality exists between the apparent fracture toughness and the square root of the notch root radius, $\rho^{1/2}$. At values of the root radius below a small critical value, the fracture toughness is insensitive to the magnitude of the notch root radius. Irwin (18) has suggested that this critical value

of the notch root radius, ρ_c, may be equal to the crack opening stretch, δ_c, where

$$\rho_c = \delta_c = \frac{4}{\pi} \frac{\mathcal{G}_{Ic}}{\sigma_{Y.S.}} \tag{14}$$

For the single-edge-notch, two-material system ρ_c would be approximately 4×10^{-5} in.

Attempts to extend and sharpen the crack by wedge opening or fatigue cracking failed. Next a razor blade was wrapped in Teflon tape except for its tip, imbedded in the adhesive, and removed after gelation. From the following table it is apparent that the razor blade crack was not adequate. This is partly due to shrinkage during resin cure and possible blunting of the crack upon removal of the blade.

Crack Tip Characterization	Crack Length (in.)	Critical Stress (psi)
sharp, natural	.25	1600
razor blade	.25	2200
saw cut	.43	2500

The sharp, natural cracks were obtained by adding arms to the specimen and propagating the crack into the primary part of the specimen by opening the arms. Using the large loading holes (Fig. 11) the specimen was then loaded until separation occurred.

Further evidence of the necessity of a sharp, natural crack is shown in Fig. 12. The upper photograph shows fracture surfaces where the fracture initiated from a sharp, natural crack while the lower photograph shows surfaces where the initial crack was sawed with a razor blade. As a result of this study, only those specimens in which natural, sharp cracks could be obtained were used.

Compliance Calibration

A compliance calibration must be performed so that the fracture results can be interpreted. This was done numerically in the previous section with the finite element

technique. The experimental compliance calibration involves the same general procedure--determining the compliance (displacement/load) over a range of crack lengths and then evaluating the compliance derivative, dC/da, over the same range of crack lengths.

The first step in the experimental compliance calibration was to measure the displacement versus load for a range of crack lengths. A region of uniform strain where a displacement gage could be attached and proper specimen alignment were considered. All of a series of strain gages mounted at a location half the distance between the crack (adhesive layer) and a large loading hole indicated approximately the same strain. Consequently, this location was chosen as a position from which to measure the deflection. Aluminum tabs, 2.5 inches in length, were bonded to the specimen at this location and a one-inch strain gage extensometer was mounted between the ends of the tabs (Fig. 13). The contact points were positioned very close to the horizontal portion of the gage to attain a very sensitive measurement of the deflection. The signal from the four-active-arm bridge circuit of the gage was displayed on a X-Y recorder with the use of a Brush bridge amplifier. The system was calibrated with a Pratt & Whitney supermicrometer. An upper limit on the load of 2000 lbs. was imposed to prevent separation of the specimen at long crack lengths. At this relatively low load, which results in a total displacement of only about 0.0015 in., the small differences in displacements due to differences in crack lengths are very difficult to measure accurately. At the lower limit of 200 lbs., the crack was extended from one length to another with the use of a hand saw with a .012" thick blade. Two typical load-displacement curves out of a total of 22 are shown in Fig. 13. The slopes of these curves were then determined by two different methods which yielded similar results. One method involved a simple manual straight-edge fit and the other involved a two-point (400 and 1400 lbs.) straight line fit. The resulting compliance values over the range of crack lengths is shown in Fig. 14.

The next step then is to determine the compliance derivative, dC/da. The moveable strip technique described previously was used again. Polynomials of orders two, four and six were fitted in a least squares manner to the compliance-crack length data and the compliance derivative was determined (Fig. 15). The sixth order polynomial tends to oscillate, the fourth order polynomial exhibits curvature in the opposite direction and the second order polynomial yields a straight line. None of these are physically realistic representations but for purposes of comparison with the finite element results, the straight line was chosen since it is the simplest and the most realistic of the three curves.

In Fig. 16 a comparison of the finite element results and the experimental compliance calibration (second order curve of Fig. 15) is illustrated. The finite element results were taken from Fig. 7 where the relative adhesive thickness, L/W, was 0.0025 since the width of the specimen was two inches. A maximum error of about 30% occurs at the end points of these curves. This difference can probably be attributed to the inaccuracies and interpretation of the experimental results. The significance of this comparison is that the experimental results substantiate and give confidence in the finite element results. Consequently, the finite element results will be used to interpret the experimental fracture tests.

Fracture Toughness Results

The single-edge-notch adhesive joint specimen was used to measure the opening mode fracture toughness. The loading arms necessary for precracking the specimen are shown in Fig. 11. For the precracking operation a 30X StereoZoom microscope was used to monitor the crack while critical crack extension loads, F, were measured. For several specimens the critical loads and the corresponding crack lengths were plotted. With the use of this plot the precrack length was easily controlled and complete separation of the specimen was avoided.

After the crack had been propagated into the specimen by precracking, it was loaded (P in Fig. 11) at a rate of 0.2 in/min. in an Instron testing machine with universal joints in the loading arms. At the critical load the crack propagated completely thru the specimen along the center of the adhesive bond (CoB). After measuring the critical crack length from the fracture surface, the finite element results (Fig. 16) were used to obtain a critical strain energy rate or fracture toughness, $\mathcal{G}_{Ic}$. For eight specimens, $\mathcal{G}_{Ic}$ ranged from 0.35 to 0.41 in-lb/in^2 with an average value of 0.37 in-lb/in^2. Using the approximation of Eq. 9, the average value of $\mathcal{G}_{Ic}$ was 0.30 in-lb/in^2.

The final precrack, from which the critical crack length was measured, and other interesting features can be observed on the fracture surfaces. The upper photograph of Fig. 17 shows the fracture surfaces at 2X magnification. The final "thumbnail" precrack can be noted as well as parabolic markings which are characteristic of polymeric fracture surfaces (19). Also, the characteristic change of the fracture surface from mirror-like to dull to very rough as the crack extends can be observed. This morphology varies with critical loads and crack lengths, i.e. with short cracks and high loads a small mirror-like region and a large, very rough region occur while the opposite is true for long cracks with low loads. The lower photograph of Fig. 17 shows a 50X view of several crack arrest lines. A further magnification (200X) of two particular crack arrest lines are shown in Fig. 18. The right photograph shows a crack arrest line followed by stable propagation to another arrest. The left photograph shows the final arrest line before complete separation of the specimen occurred.

Before the single-edge-notch adhesive joint specimens were tested, tapered (7^o) double cantilever beam (DCB) specimens (Fig. 19) were tested to determine if the specimen preparation was adequate and to establish the fracture toughness for the

adhesive system used throughout the study. This specimen geometry, the same as that used by Ripling and Mostovoy (9), allows for good crack propagation stability since the crack runs for only a short distance and then arrests. By proper tapering of the specimen, the compliance derivative, which has been determined for this two-material specimen (9), is a constant so that only the critical load need be known to determine the fracture toughness. Figure 19 shows typical results from one specimen where the peaks represent the critical loads for crack extension and the valleys represent crack arrest. The average $\mathcal{G}_{Ic}$ for several specimens was 0.35 in-lb/in^2, while Ripling and Mostovoy obtained an average value of 0.33 in-lb/in^2.

To test the feasibility of applying one-material fracture mechanics results to two-material adhesive systems, a two-material, tapered (16^o) DCB specimen was tested and the results analyzed using one-material results previously obtained (16). From 14 values obtained from three specimens, an average value of $\mathcal{G}_{Ic}$ of .35 in-lb/in^2 was computed. This agrees well with results previously reported in this paper for the same adhesive system. The following table summarizes the results for the fracture toughness of the adhesive system. Complete results are shown in Table 1.

Source	$\mathcal{G}_{Ic}$ (in-lb/in^2)
Ref. 10	.33
7^o DCB	.35
16^o DCB	.35
Single-Edge-Notch	.37

SUMMARY AND CONCLUSIONS

The problem of applying fracture mechanics to the tensile mode of crack extension in an adhesive bonded system was examined. An aluminum-epoxy-aluminum plate with a sharp single-edge-crack in the epoxy layer was considered.

The finite element method was used to determine stress intensity factors, K, and strain energy rates, $\mathcal{G}$. A radial array of elements with a small hole at the crack tip (Fig. 4) is an effective grid system for fracture mechanics problems. For evaluating K, the finite element displacement method appears adequate although an extrapolation is necessary. The finite element compliance method is an accurate computational method for determining $\mathcal{G}$ over a wide range of crack lengths.

An experimental compliance calibration for the single-edge-notch two-material plate was made; adequate accuracy was very difficult to obtain due to the limit on the applied load and consequently the small differences in displacements at different crack lengths. A great deal of care and cleanliness in the specimen preparation is essential in order to attain a good bond. For the adhesive system a very sharp, natural crack tip is necessary for the measurement of a minimum fracture toughness.

The following conclusions can be enumerated:

1. For the two-material system (Fig. 2), $\mathcal{G}$ decreases as the adhesive layer becomes thinner. For a very thin adhesive layer, $\mathcal{G}_{\text{Al-Ep}}$ for the two-material plate (aluminum-epoxy) is approximately equal to $\mathcal{G}_{\text{Al}}$ for the one-material system. This conclusion is based on finite element results. This appears to be a valid conclusion for any adhesive system with a very thin adhesive layer containing a crack. Indeed, the fracture toughness values evaluated with the 16° tapered DCB specimen by using this approximation agree well with the results of Ref. 10.

2. For the two-material system:

$$K^2_{\text{Al-Ep}} = \mathcal{G}_{\text{Al-Ep}} E_{\text{Ep}}$$

where E_{Ep} is the modulus of the adhesive (epoxy).

3. For a very thin adhesive layer:

$$\frac{K^2_{\text{Al}}}{K^2_{\text{Al-Ep}}} \simeq \frac{E_{\text{Al}}}{E_{\text{Ep}}}$$

4. Good reproducibility of the fracture toughness values measured for the two-material system by using a single-edge-notch plate and tapered double cantilever beam specimens indicates the geometry independence of the fracture toughness.

REFERENCES

1. A. A. Griffith, "The Phenomena of Rupture and Flow in Solids," Phil. Trans. Roy. Soc., 1920, pp. 163-198.

2. G. R. Irwin, "Fracturing of Metals," American Society of Metals, pp. 147-166, 1948.

3. S. Mostovoy and E. J. Ripling, "Fracture Toughness of an Epoxy System," Journal of Applied Polymer Science, Vol. 10, 1966, pp. 1351-1371.

4. P. C. Paris and G. C. Sih, "Stress Analysis of Cracks," Fracture Toughness Testing and its Applications, ASTM STP No. 381, 1965.

5. W. B. Fichter, "Stresses at the Tip of a Longitudinal Crack in a Plate Strip," NASA TR R-265, 1967.

6. W. G. Knauss, "Stresses in an Infinite Strip Containing a Semi-Infinite Crack," Journal of Applied Mechanics, Transactions of the ASME, 1966, pp. 356-362.

7. E. J. Ripling, S. Mostovoy and R. L. Patrick, "Application of Fracture Mechanics to Adhesive Joints," ASTM STP No. 360, Symposium on Recent Developments in Adhesion Science, 1963.

8. E. J. Ripling, S. Mostovoy and R. L. Patrick, "Measuring Fracture Toughness of Adhesive Joints," Materials Research and Standards, ASTM, Vol. 4, No. 3, March, 1964.

9. S. Mostovoy and E. J. Ripling, "Influence of Water on Stress Corrosion Cracking of Epoxy Bonds," Journal of Applied Polymer Science, Vol. 13, 1969, pp. 1083-1111.

10. S. Mostovoy, C. Bersch and E. J. Ripling, "Fracture Toughness of Adhesive Joints," National SAMPE Technical Conference, Aerospace Adhesives and Elastomers, Dallas, October 6-8, 1970, pp. 273-286, Vol. 2.

11. O. C. Zienkiewicz, The Finite Element Method in Structural and Continum Mechanics, McGraw-Hill, 1967.

12. S. K. Chan, I. S. Tuba and W. K. Wilson, "On the Finite Element Method in Linear Fracture Mechanics," Engineering Fracture Mechanics, Vol. 2, 1970, pp. 1-17.

13. A. S. Kobayashi, D. E. Maiden, B. J. Simon and S. Iida, "Application of Finite Element Analysis Method to Two-Dimensional Problems in Fracture Mechanics," ASME Paper No. 69-WA/PVP-12, 1969.

14. R. K. Leverenz, "A Finite Element Stress Analysis of a Crack in a Bi-Material Plate," University of Illinois, T&AM Report No. 331, June 1970, to be published in the International Journal of Fracture Mechanics.

15. J. P. Gallagher, "Experimentally Determined Stress Intensity Factors for Several Contoured Double Cantilever Beam Specimens," presented at the Second National Symposium on Fracture Mechanics, June 1968.

16. E. Gross, J. E. Srawley and W. F. Brown, "Stress-Intensity Factors for a Single-Edge-Notch Tension Specimen by Boundary Collocation of a Stress Function," NASA TN D-2395, 1964.

17. J. H. Mulherin, D. F. Armiento and H. Markus, "The Relationship Between Fracture Toughness and Stress Concentration Factors for Several High-Strength Aluminum Alloys," Journal of Basic Engineering, Transactions of the ASME, 1964, pp. 709-717.

18. G. R. Irwin, "Trends in Fracture Mechanics," ASM Fracture Control Conference, Philadelphia, Pennsylvania, January, 1970.

19. C. E. Feltner, "On the Mechanical Behavior and Fracture Morphology of Epoxy Resin," University of Illinois, T&AM Report No. 224, August 1962.

TABLE 1. FRACTURE TOUGHNESS OF THE ADHESIVE SYSTEM

SEN			7^{o} DCB	16^{o} DCB
Crack Length, in.	Load, lbs.	$\mathcal{G}_{Ic}$, in-lb/in^2	$\mathcal{G}_{Ic}$, in-lb/in^2	$\mathcal{G}_{Ic}$, in-lb/in^2
.12	2680	.41	.32	.34
.16	2100	.35	.33	.35
.18	2100	.40	.35	.36
.20	1900	.37	.35	.37
.25	1620	.37	.35	.36
.25	1620	.37	.35	.37
.28	1460	.35	.35	.37
.32	1340	.36	.35	.38
			.37	.40
			.39	.33
			.39	.33
			.32	.32
			.33	.33
			.35	.34
			.37	
AVERAGE $\mathcal{G}_{Ic}$		.37	.35	.35

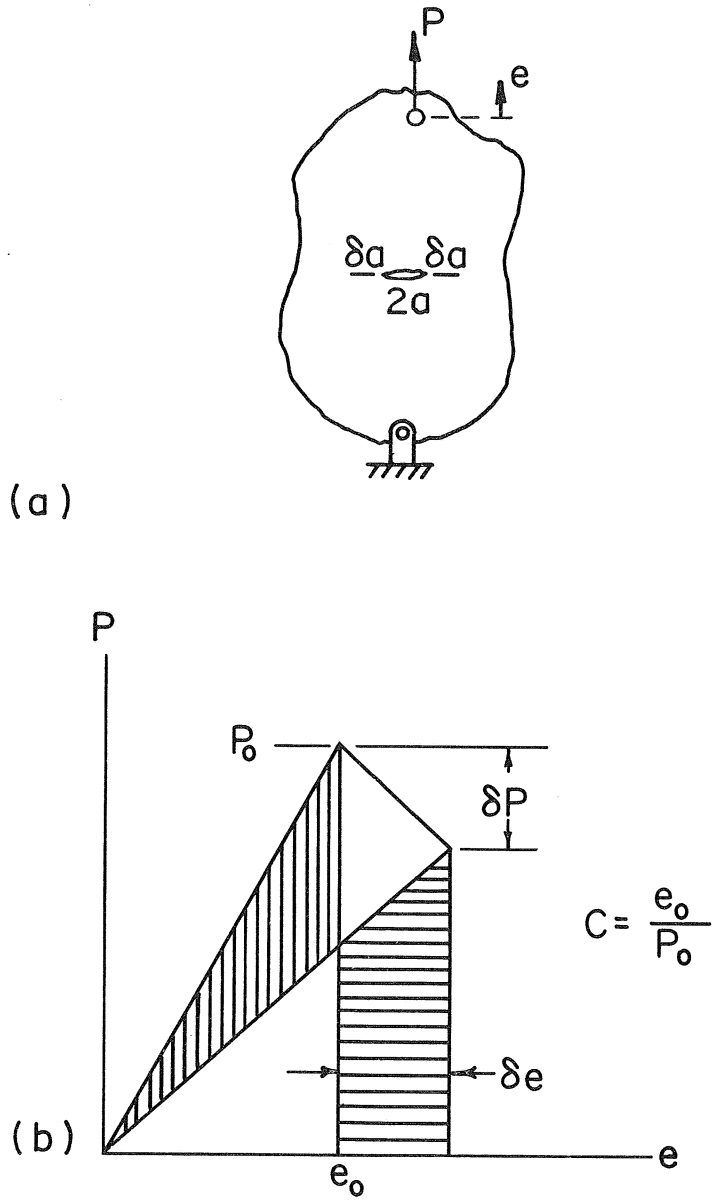

Fig. 1 (a) Loaded Body Containing a Crack

(b) Load – Displacement Diagram of a Cracked Body Experiencing an Increment of Crack Extension

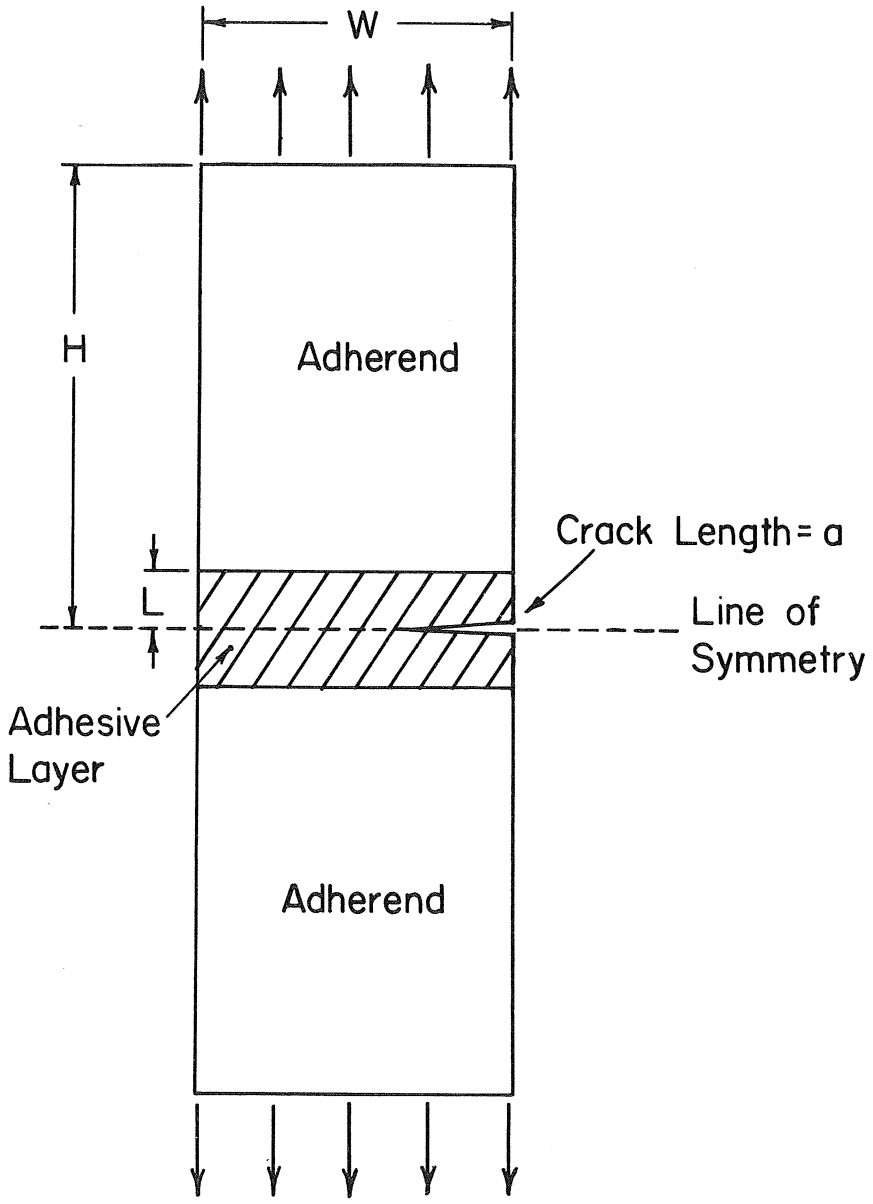

Fig. 2 Single-Edge-Notch Two-Material Plate

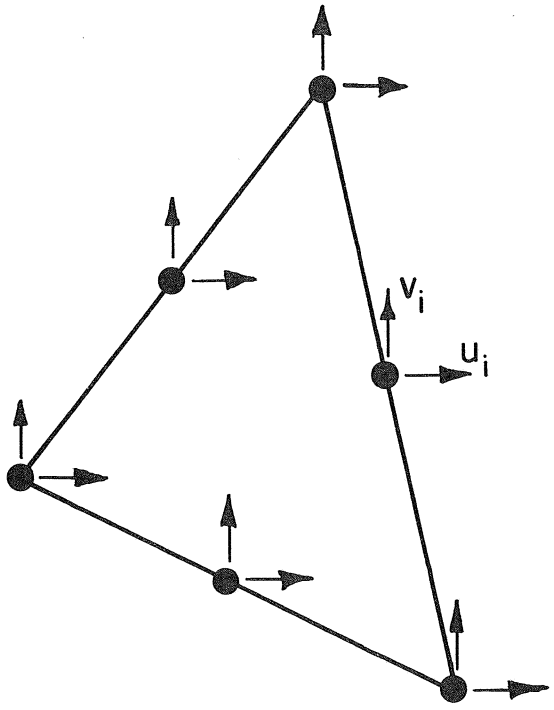

Fig. 3 Triangular Element With Six Nodes Used in Finite Element Analysis

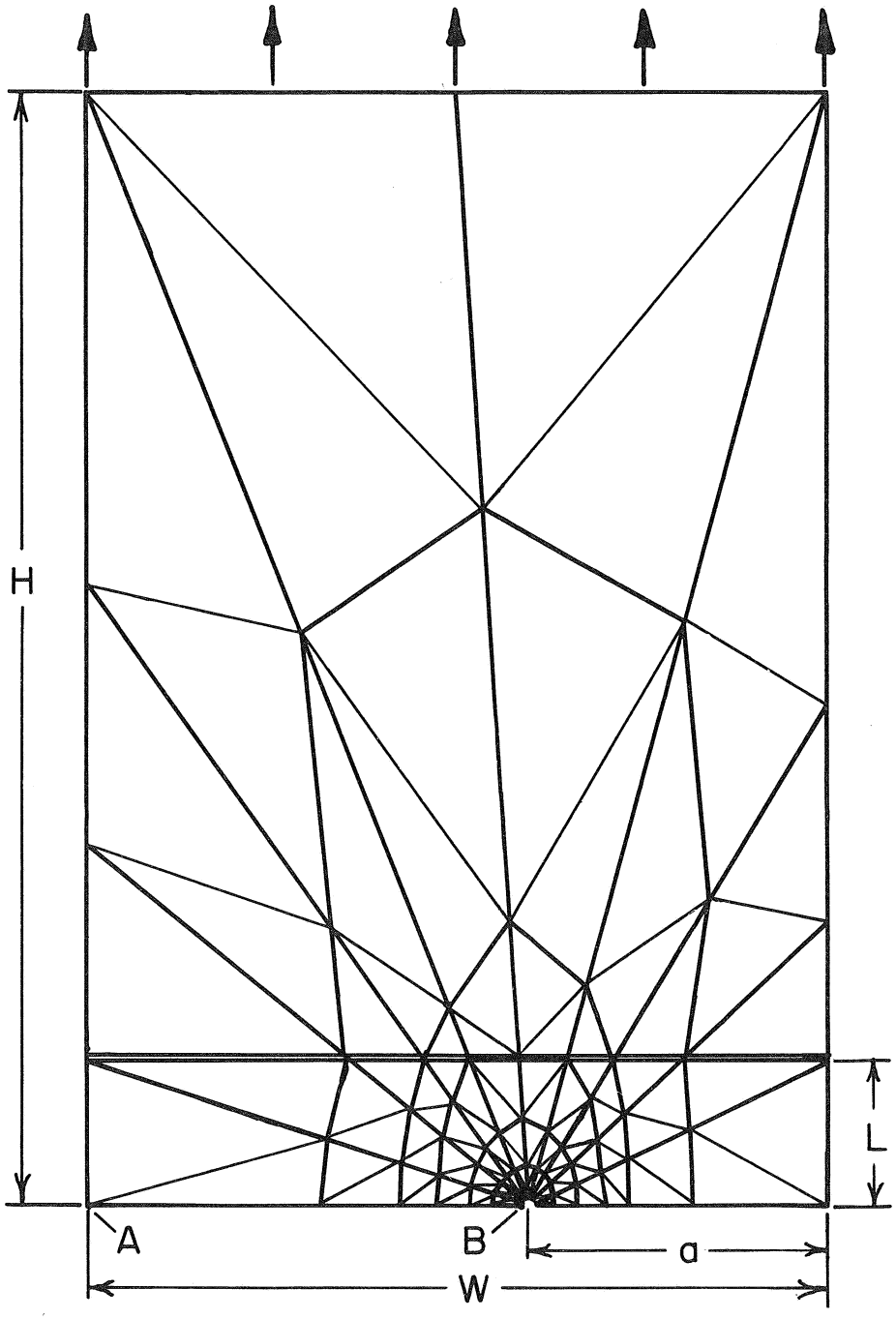

Fig. 4 Finite Element Grid Pattern (Not to Scale)

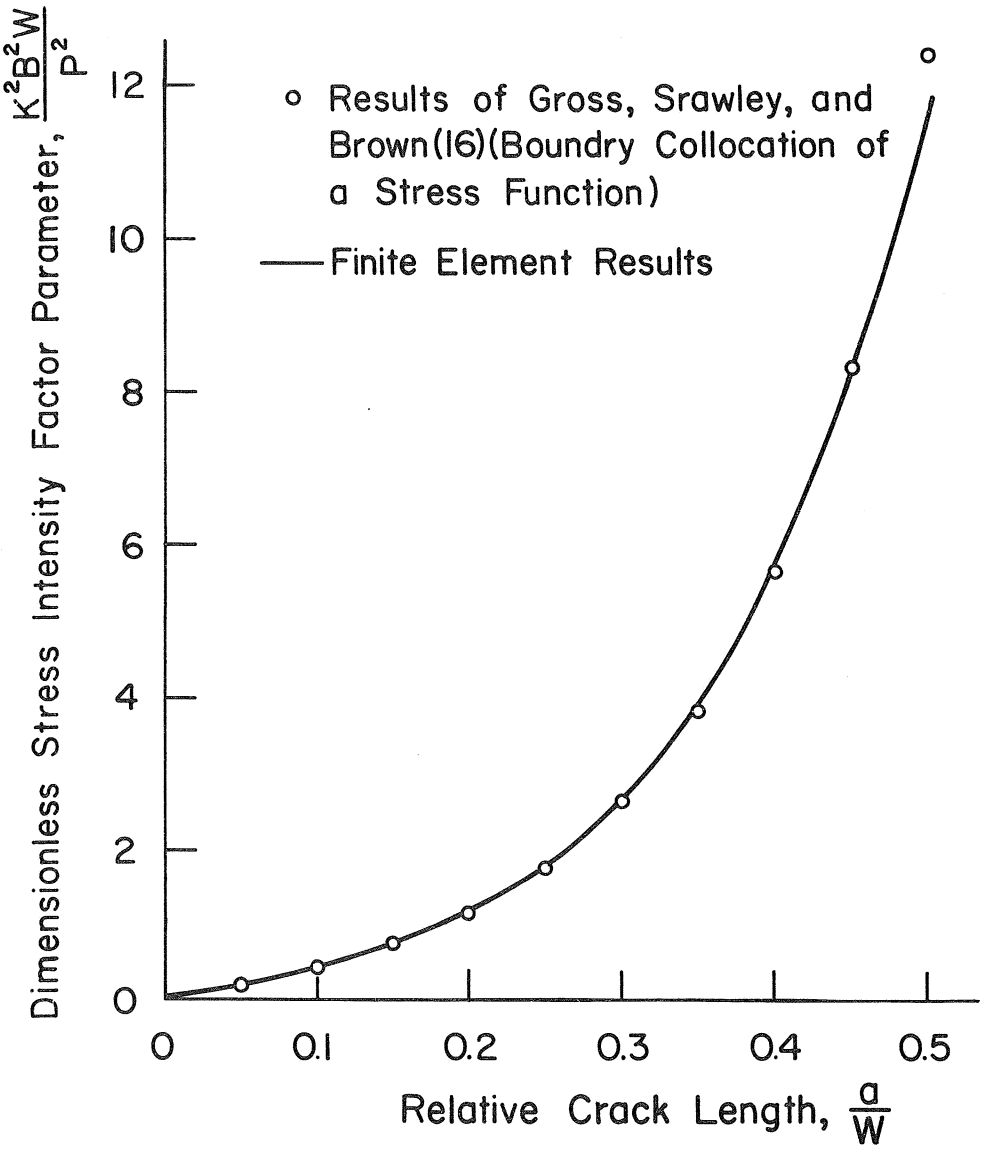

Fig. 5 Stress Intensity Factors, K, for One-Material, Single-Edge-Notch Plate

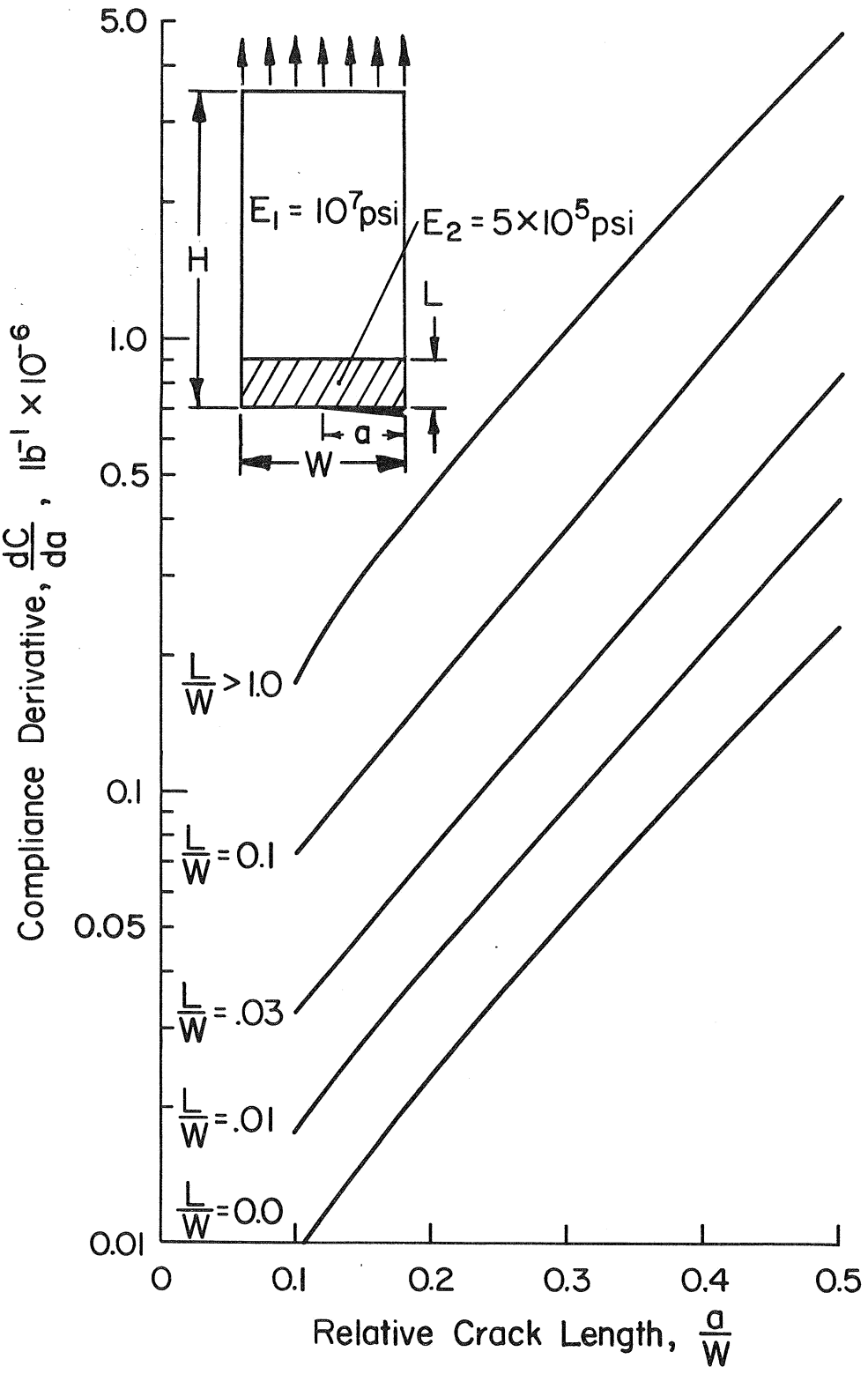

Fig. 6 Compliance Derivative as a Function of Crack Length at Various Adhesive Thicknesses From Finite Element Analysis

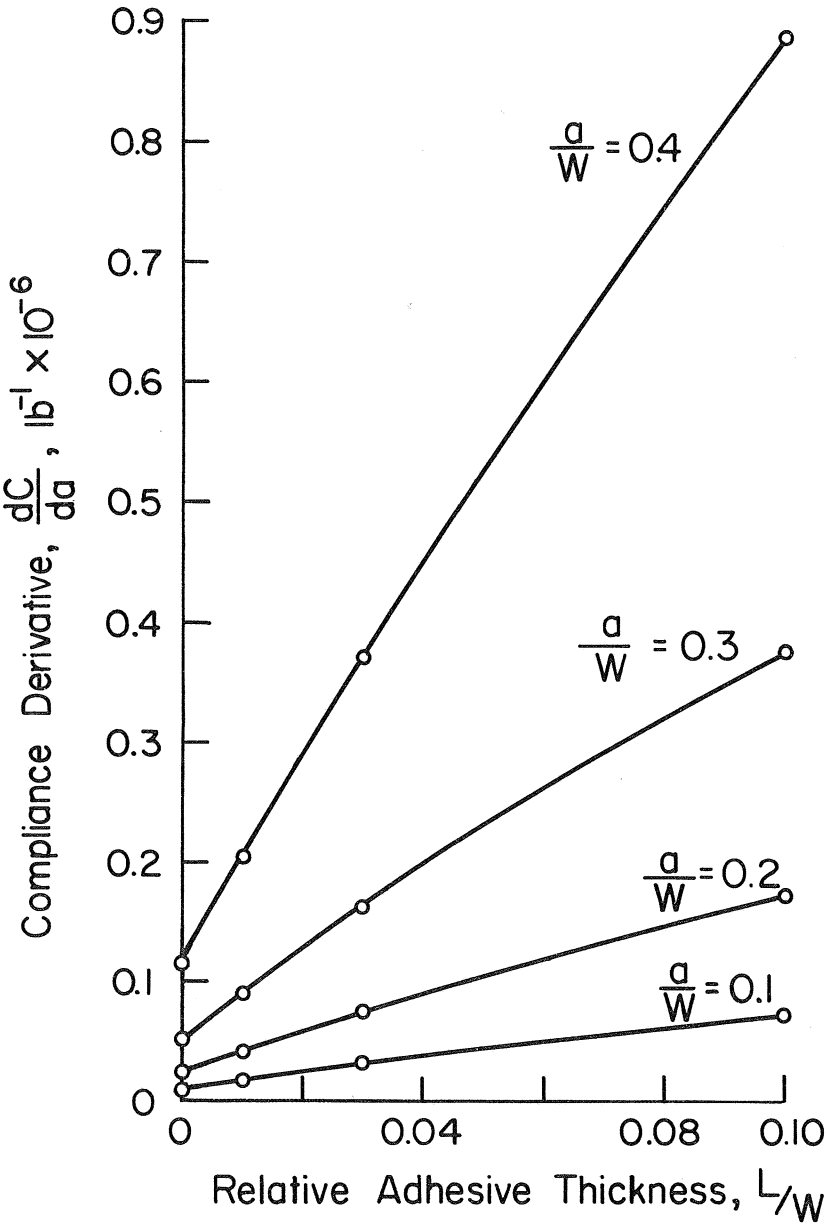

Fig. 7 Compliance Derivative as a Function of Adhesive Thickness at Various Crack Lengths From Finite Element Analysis

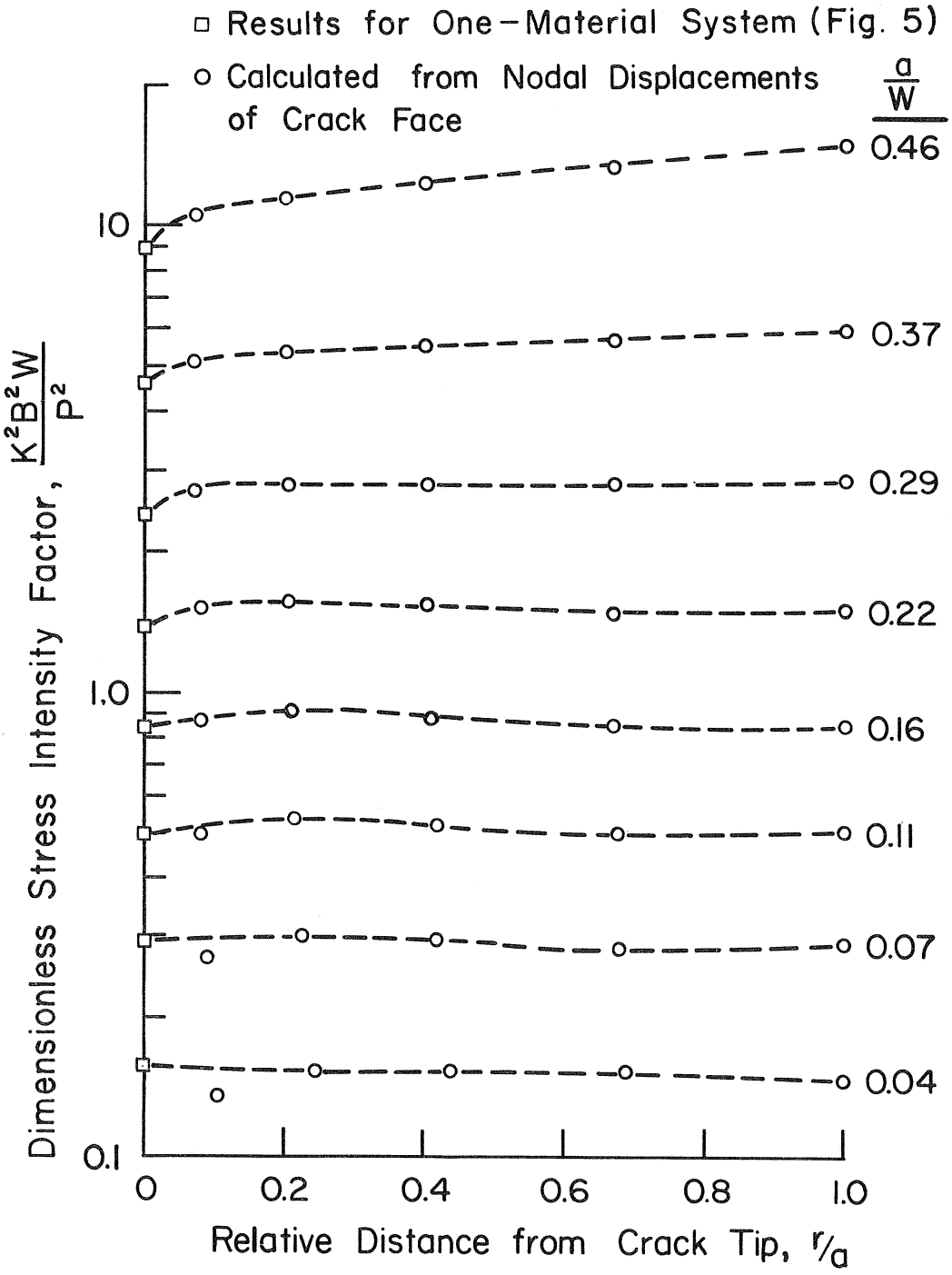

Fig. 8 Displacement Method Extrapolation Procedure to Determine Stress Intensity Factors - One Material System

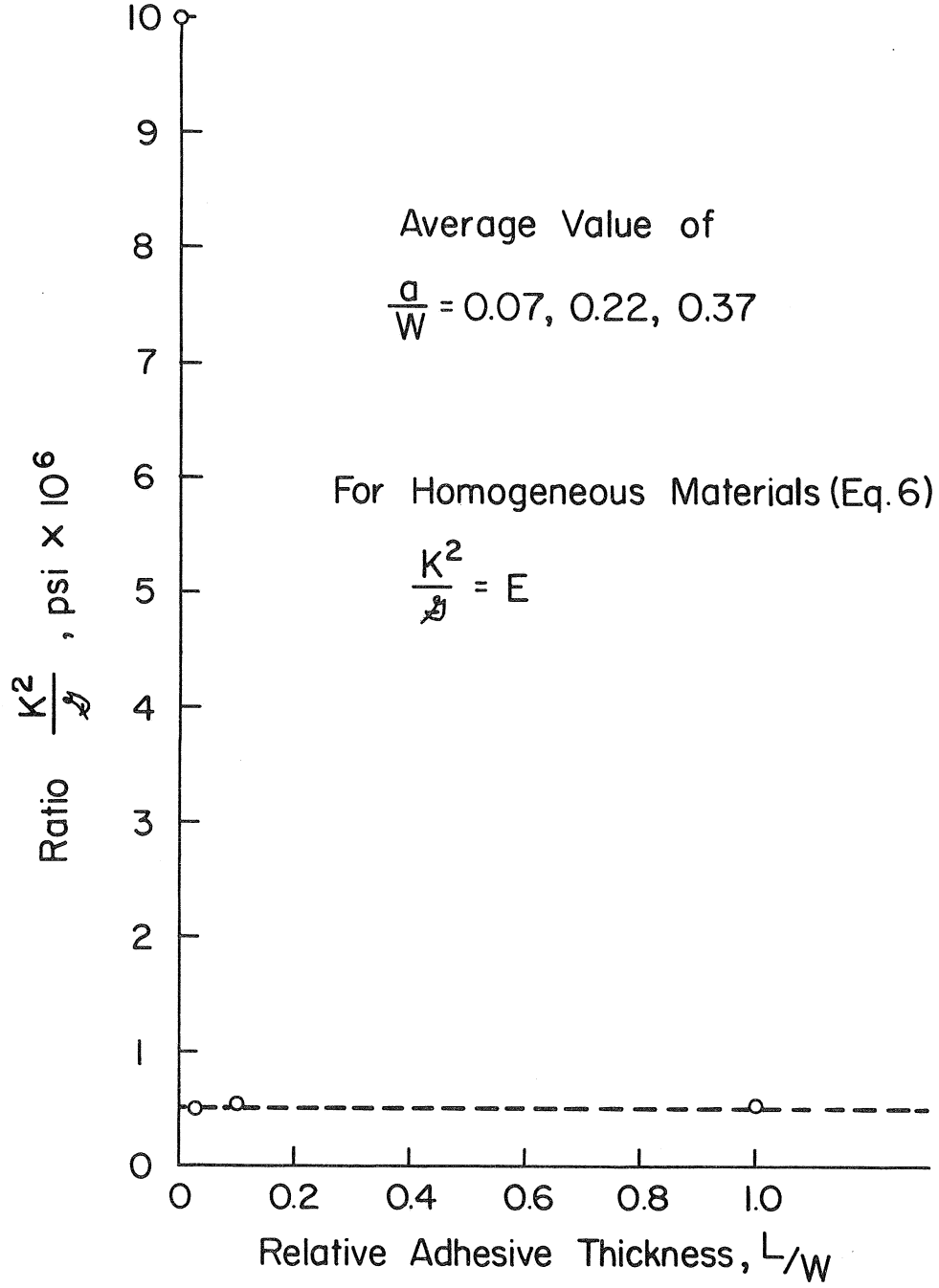

Fig. 9 Ratio $\frac{K^2}{\mathcal{G}}$ as a Function of Adhesive Thickness

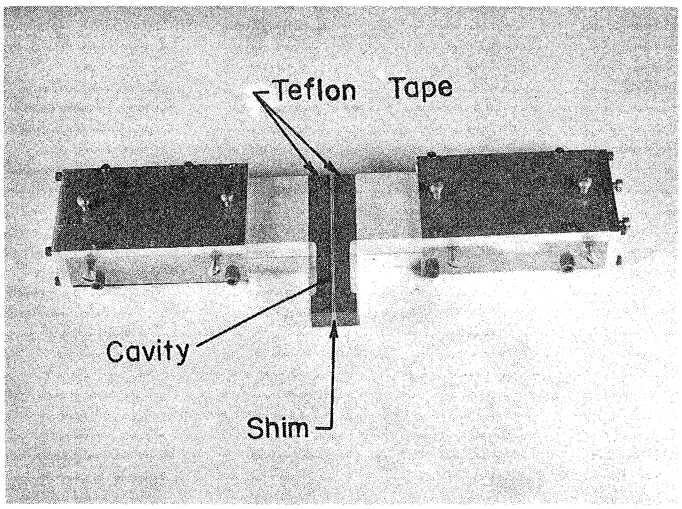

Fig. 10 Fixture for Holding Adherends During Preparation

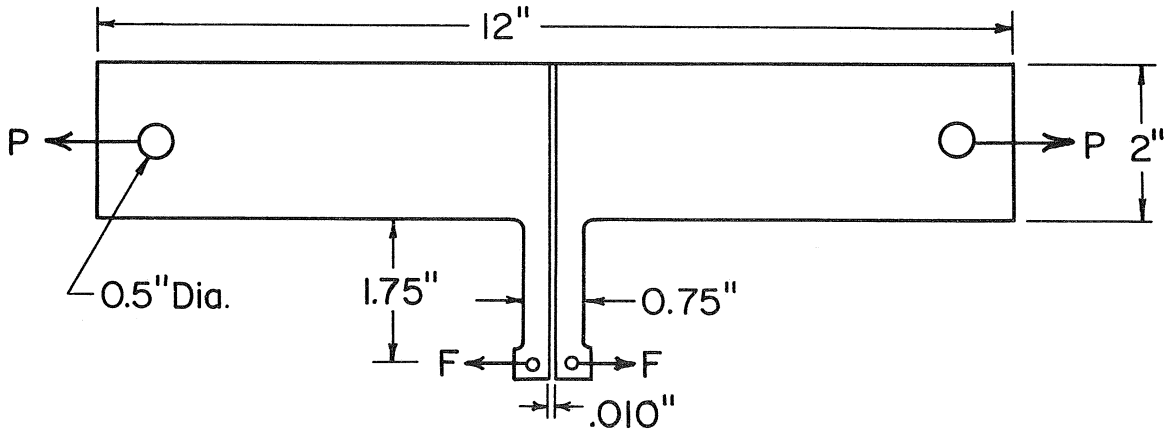

Fig. 11 Single-Edge-Notch Specimen

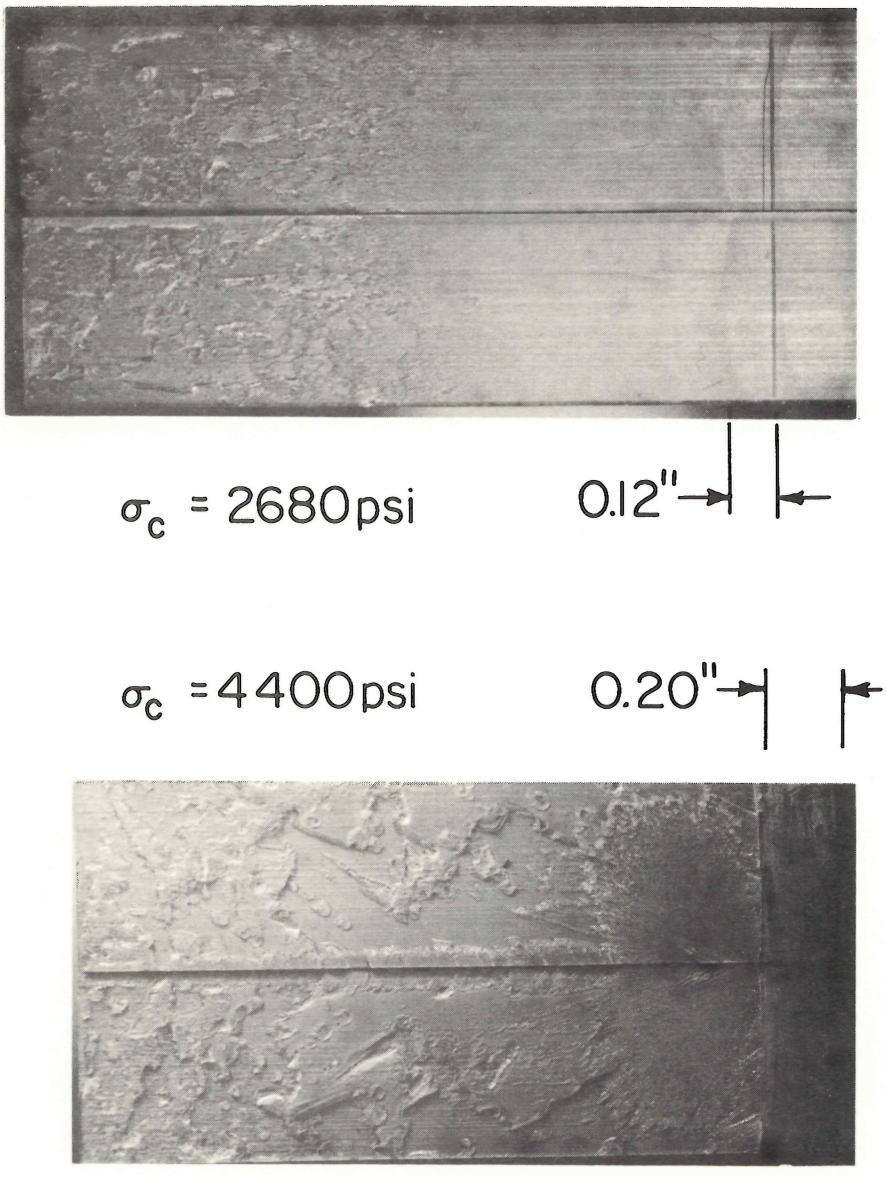

Fig. 12 Differences in Fracture Surfaces Due to Type of Precrack

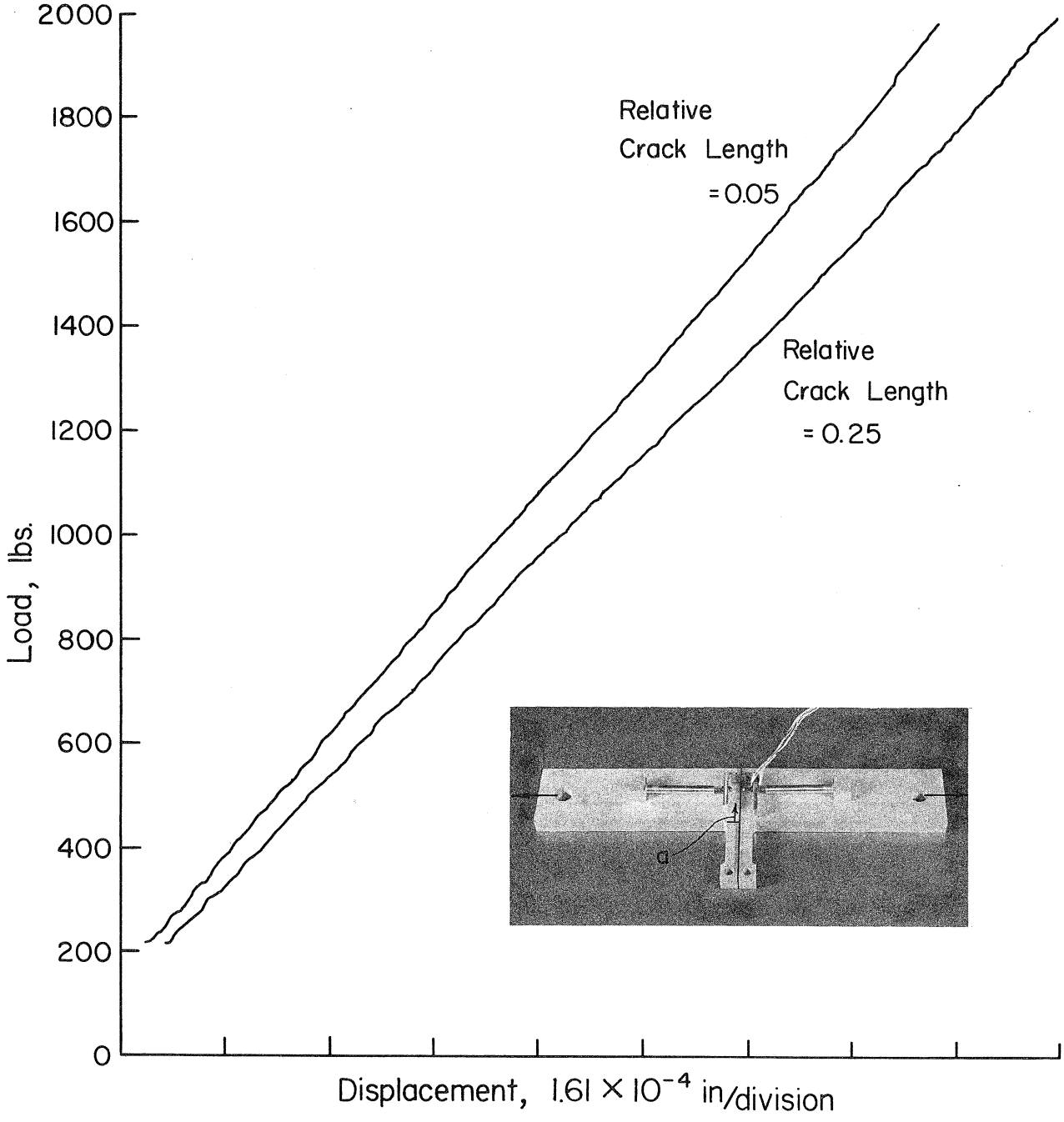

Fig. 13 Load Vs. Displacement for Two Typical Crack Lengths

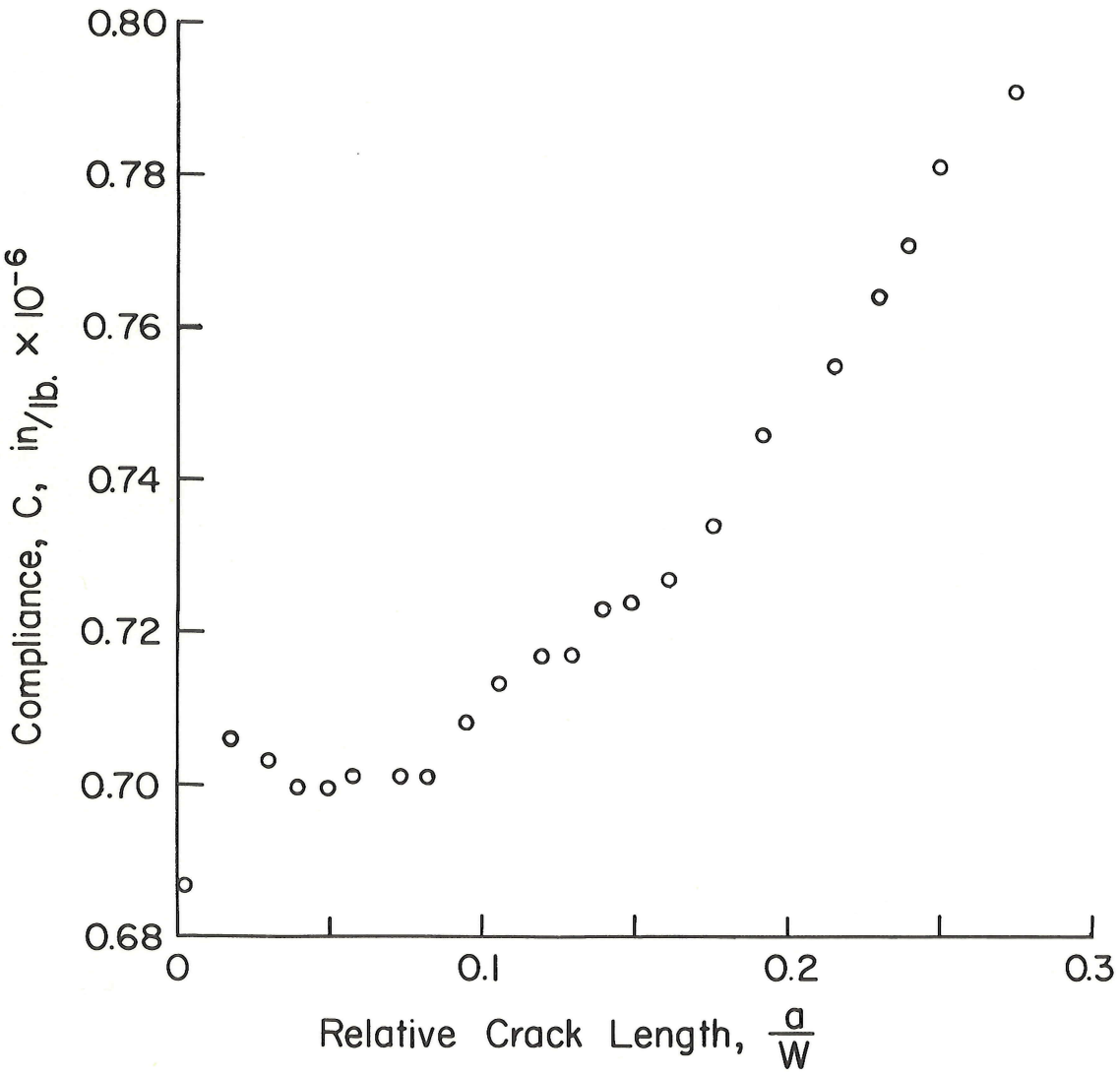

Fig. 14 Experimental Compliance Values over a Range of Crack Lengths

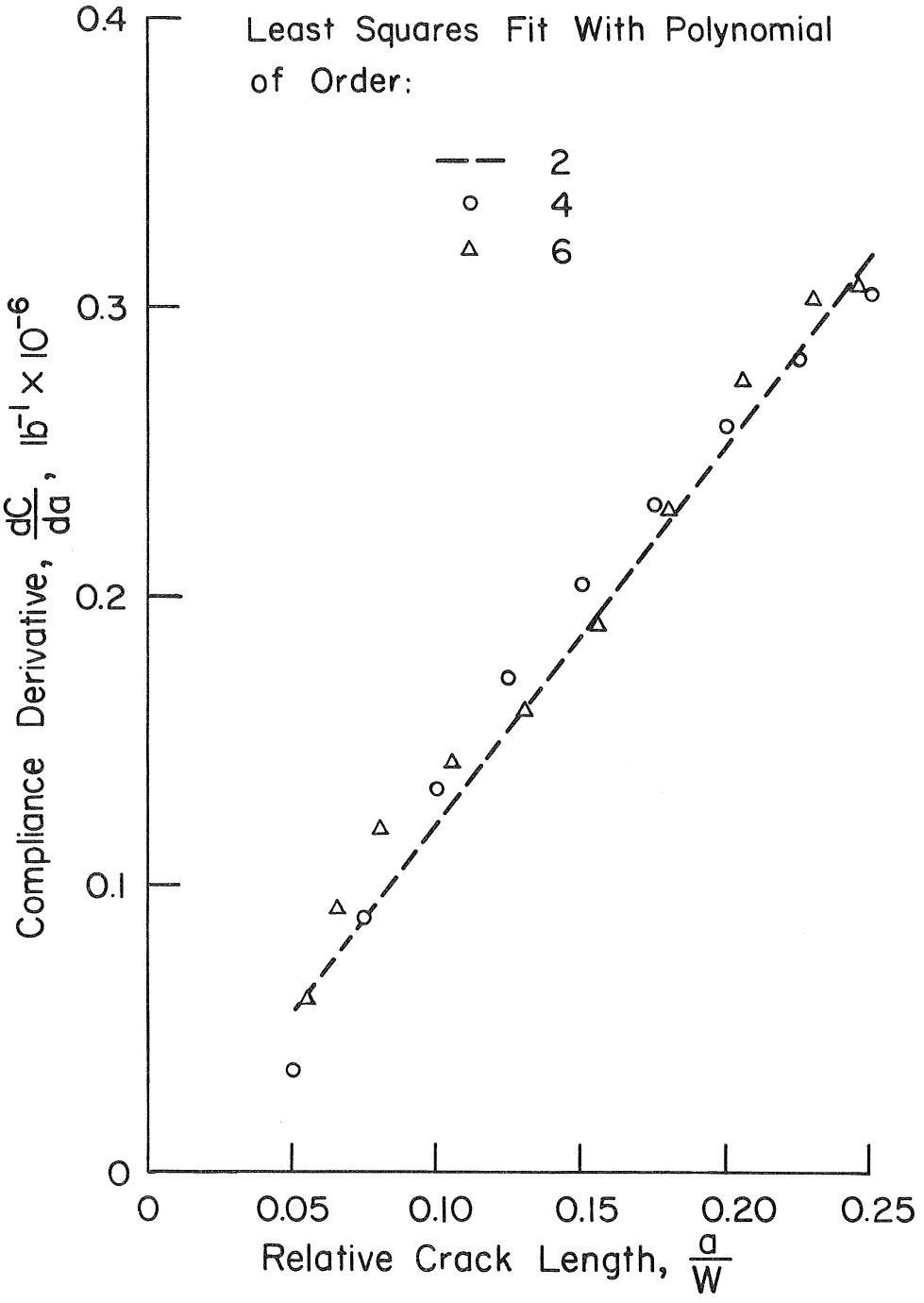

Fig. 15 Compliance Derivative at Various Crack Lengths Based on Experimental Measurements

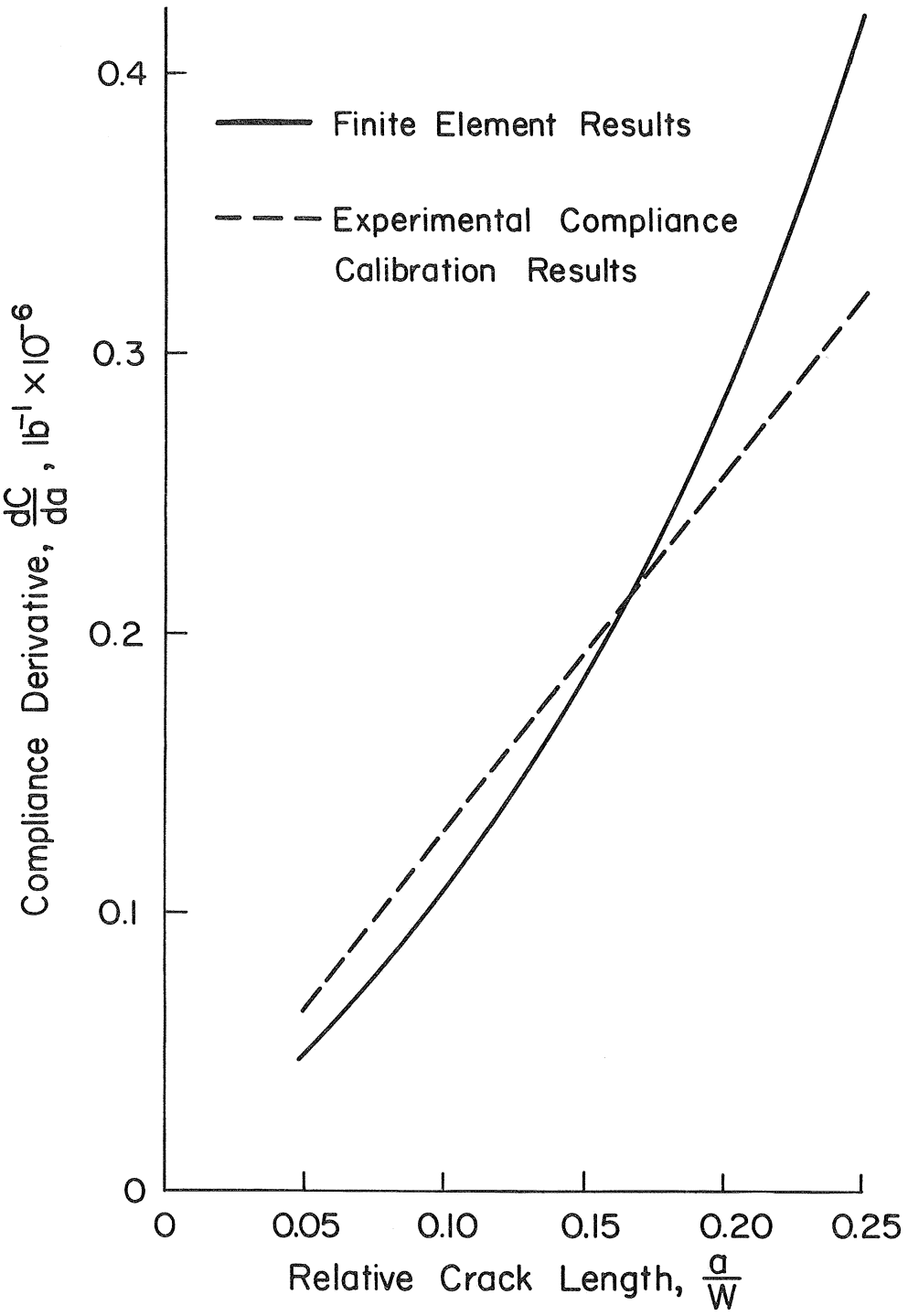

Fig. 16 Comparison of Numerical and Experimental Compliance Results

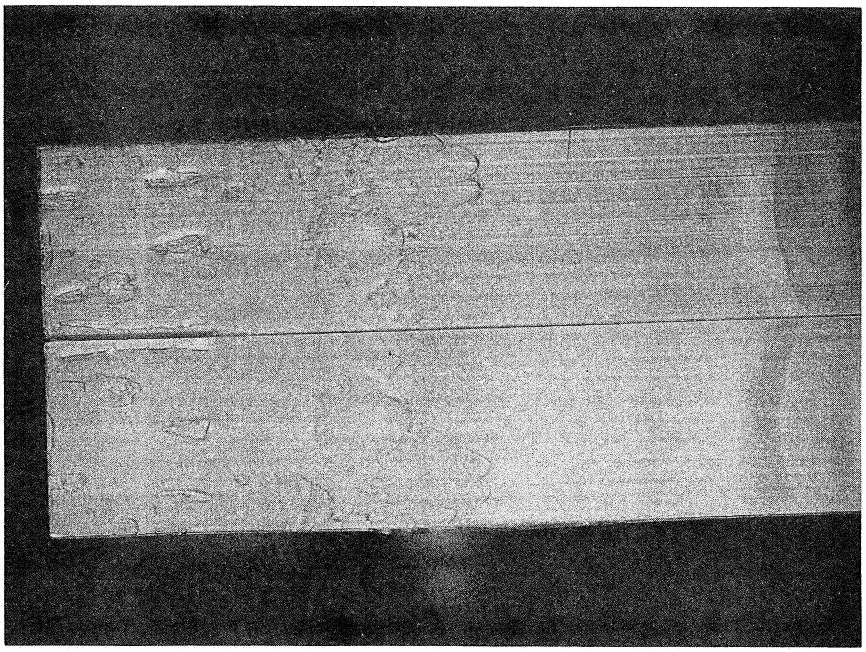

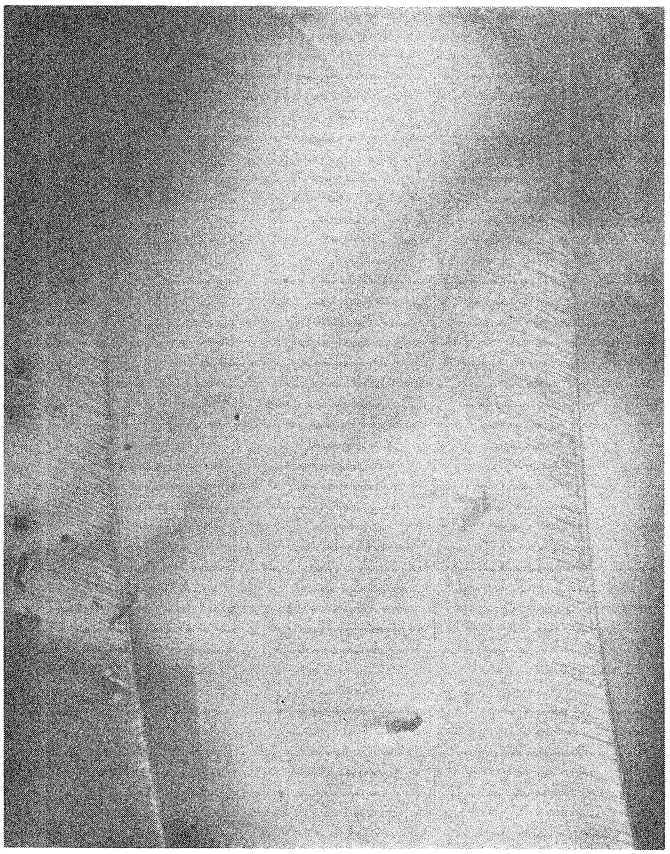

Fig. 17 Fracture Surfaces (2X and 50X)

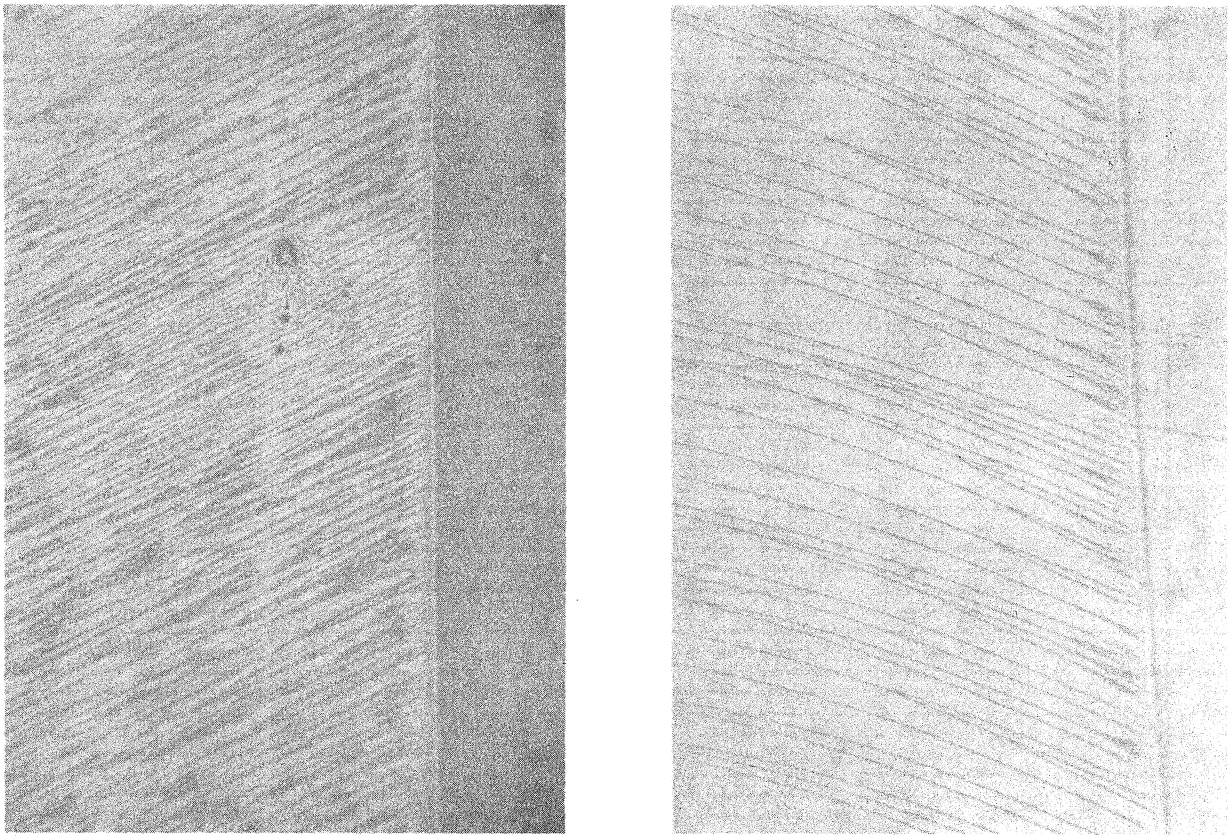

Fig. 18 Crack Arrest Lines on Fracture Surfaces (200X)

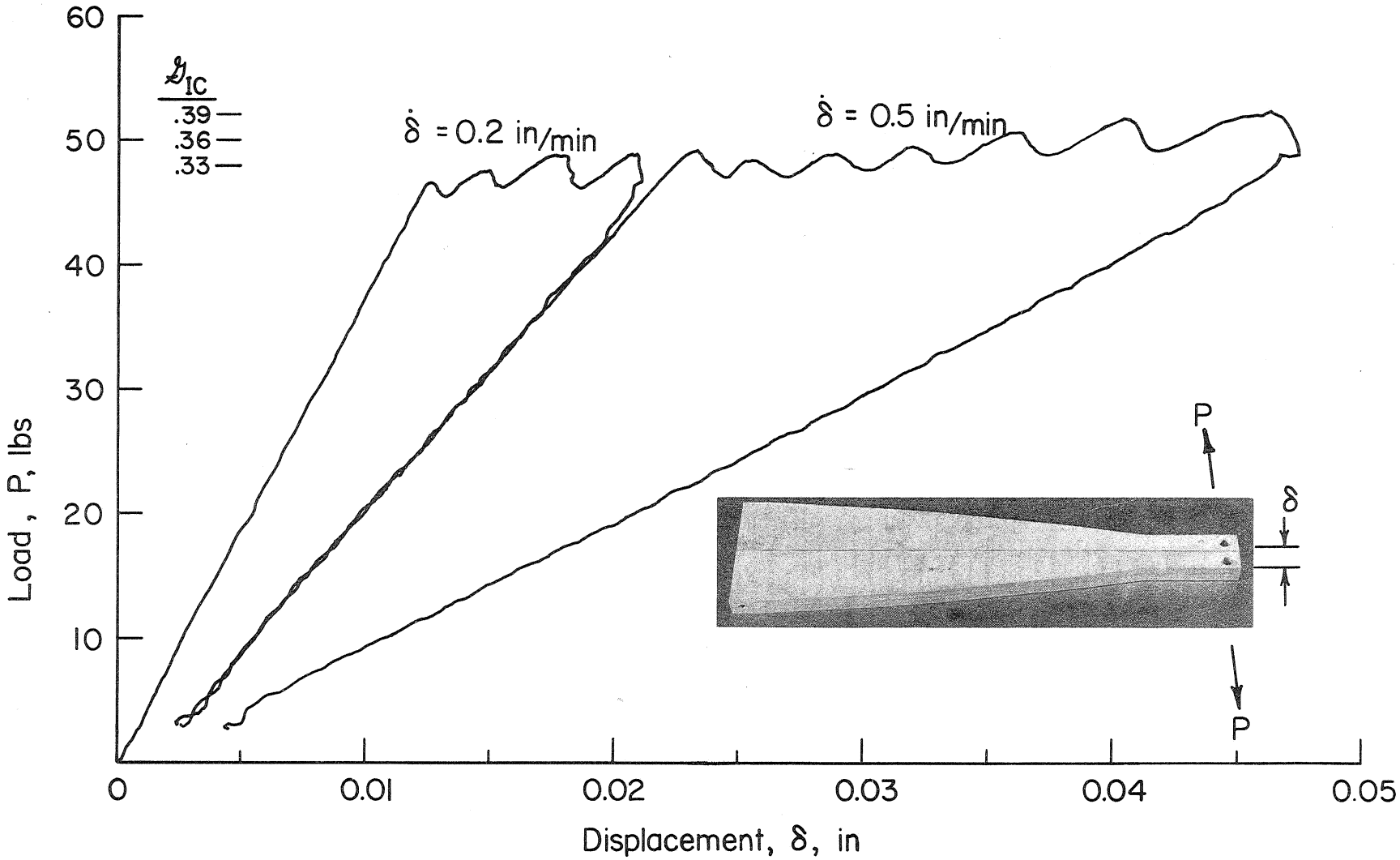

Fig. 19 Increasing Load Record for Tapered (7°) DCB Specimen

Distribution List for Contract N00019-69-C-0289

with Department of Theoretical and Applied Mechanics, University of Illinois

	No. of Copies
1. AIR-52032A Naval Air Systems Command Washington, D. C. 20360	5
2. Naval Research Laboratory Washington, D. C. 20390 Code 6100 1 Copy Code 6120 1 Copy Code 8430 1 Copy Code 8433 1 Copy	4
3. Naval Ordnance Laboratory White Oak, Maryland 20910 Attention: Code 234	1
4. Naval Ship Engineering Center Washington, D. C. 20360 Attention: Code 6101E	1
5. Naval Ship R & D Center Anapolis, Maryland	1
6. Naval Ship R & D Center Washington, D. C. 20007 Attention: Code 725	1
7. Chief of Naval Research Washington, D. C. 20360	1
8. Materials Research Laboratory, Inc. One Science Road Glenwood, Illinois 60425	1
9. Alpha R & D Inc. 14323 So. Western Avenue Blue Island, Illinois 60406	1
10. ORD-0333A Naval Ordnance Systems Command Washington, D. C. 20360	1

Distribution List for Contract N00019-69-C-0289

with Department of Theoretical and Applied Mechanics, University of Illinois

		No. of Copies
20.	Solar Aircraft Co. 2200 Pacific Highway San Diego, California 92112 Attention: Dr. A. G. Metcalfe	1
21.	Professor John Outwater University of Vermont Burlington, Vermont 05401	1
22.	Hughes Aircraft Co. Aerospace Group R & D Division Culver City, California 90130	1
23.	General Electric Co. Manufacturing Engineering Services One River Road Schenectady, New York 12305	1
24.	A. O. Smith Co. Milwaukee, Wisconsin 53201	1
25.	Mr. W. Cox Dr. S. Brelant Aerojet-General Corporation P. O. Box 296 Azusa, California 91702	1
26.	IIT Research Institute Technology Center 10 West 35th Street Chicago, Illinois 60616	1
27.	Owens-Corning Fiberglas Corporation (Mr. R. J. Weaver) 806 Connecticut Avenue, N. W. Washington, D. C. 20015	1
28.	PPG Industries 7801 Norfolk Avenue Room 201 Bethesda, Maryland 20014	1

Distribution List for Contract N00019-69-C-0289

with Department of Theoretical and Applied Mechanics, University of Illinois

		No. of Copies
38.	Prof. F. McGarry Massachusetts Institute of Technology Cambridge, Massachusetts 02139	1
39.	Space Sciences Laboratory General Electric Co. P. O. Box 8555 Philadelphia, Pennsylvania 19101	1
40.	Avco Corporation Lowell Industrial Park Lowell,Massachusetts 01851	1
41.	Arthur D. Little, Inc. Acorn Park Cambridge, Massachusetts 02140 Attention: Stephen L. Kaplan	1
42.	Dr.Robert R. Stromberg National Bureau of Standards Washington, D. C. 20234	1
43.	Research Department Dow Corning Corporation Midland, Michigan 48640 Attention: Dr. O. K. Johannson	1
44.	NASA Headquarters Washington, D. C. 20546 Attention: N. Mayer (RV-2) B. Achhammer (RRM)	2
45.	Lewis Research Center NASA 21000 Brookpark Road Cleveland, Ohio 44135 Attention: Materials and Structures Div. Chemical Systems Division Liquid Rocket Technology Branch	3
46.	HITCO 1600 W. 135th St. Gardena, California 90249	1

Distribution List for Contract N00019-69-C-0289

with Department of Theoretical and Applied Mechanics, University of Illinois

		No. of Copies
56.	Research Center General Precision Inc. 1150 McBride Avenue Little Falls, New Jersey 07424 Attention: Dr. J. L. Rutherford	1
57.	Plastics and Packaging Laboratory Feltman Research Laboratory Picatinny Arsenal Dover, New Jersey 07801 (Attn: Mr. Bodnar)	1
58.	Naval Air Systems Command Washington, D. C. 20360 Attention: AIR-604 (Incl. 15 for DDC)	17
59.	Dr. A. Kremheller Department 72-14 Zone 402 Lockheed-Georgia Company Marietta, Georgia 30060	1
60.	TRW Equipment Laboratories TRW Inc. 23555 Euclid Avenue Cleveland, Ohio 44117	1
61.	Hercules Research Center Wilmington, Delaware 19899 Attention: J. T. Paul	1
62.	Bell Telephone Laboratories, Inc. Murry Hill, New Jersey 07971 Attention: R. Sabia	1
63.	Prof. James L. Lubkin Department of Civil Engineering Michigan State University East Lansing, Michigan 48823	1
64.	University of California Forest Products Laboratory 1301 South 46 Street Richmond, California 94801 Attention: J. Marian	1